JOURNAL OF AIRCRAFT
Vol. 31, No. 1, Jan.–Feb. 1994

Method for the Prediction of Wing Maximum Lift

Walter O. Valarezo* and Vincent D. Chin†
McDonnell Douglas Aerospace, Long Beach, California 90846

This article describes the development of a semiempirical three-dimensional method for the prediction of maximum lift for complex multielement wing geometries. The method is a combination of cost effective and reliable CFD technology (a surface panel method), and an empirically observed phenomenon occurring at maximum lift conditions that is introduced here as the pressure difference rule. The panel method solutions used in conjunction with the pressure difference rule yield surprisingly accurate predictions of maximum lift for both clean wings as well as multielement wings. Comparisons with experimental data are presented for increasingly complex high-lift wing geometries including full transport aircraft configured for landing.

Nomenclature

$C_{L\,\max}$ = maximum lift coefficient
C_p = surface pressure coefficient
C_p^* = critical pressure coefficient
$C_{p\,\text{peak}}$ = suction peak coefficient
$C_{p\,\text{te}}$ = pressure coefficient at trailing edge
M_∞ = freestream Mach number
R_N = Reynolds number based on local chord
δ_f = flap deflection angle, deg
δ_s = slat deflection angle, deg
η = nondimensional spanwise wing station

Introduction

WITH the advent of highly efficient transonic wing designs there has been renewed interest in more efficient high-lift wing designs. New-generation wing designs are able to generate a higher cruise lift coefficient (at a given drag level) than the more conventional designs of the past. Hence, a required lift force as dictated by the mission can be achieved with less wing area than previously possible. A reduction in wing area has an adverse impact on the high-lift system, because it too will be required to efficiently generate very high-lift coefficients to achieve needed performance requirements during any of the phases where the high-lift system is deployed.

An aerodynamically simple solution would be to increase the complexity of the high-lift system to achieve very high-lift coefficients, e.g., by increasing the number of elements of the high-lift wing (flaps in particular), by introducing exotic actuation motions, or by incorporating power effects. However, the commercial transport sector equates simplicity with reduced cost and improved reliability and maintainability. Hence, the trend has been to reduce the number of elements and to generate the necessary high-lift levels by properly designing the aerodynamic surfaces and configuring the aircraft at its optimum for the mission. While much of the aerodynamic design task can now be performed numerically for the clean wing at transonic conditions (at least for attached flow situations), corresponding methods for high-lift configuration analysis have lagged far behind.

Presented as Paper 92-0401 at the 30th Aerospace Sciences Meeting and Exhibit, Reno, NV, Jan. 6–9, 1992; received Feb. 19, 1992; revision received Aug. 24, 1992; accepted for publication Oct. 28, 1992.

*Principal Specialist, Aerodynamics Technology. Senior Member AIAA.
†Senior Engineer, Aerodynamics Technology. Member AIAA.

As illustrated in Fig. 1, the flow about multielement airfoils configured for high lift is very complex and does not lend itself yet to pure computation by any method reported in the open literature. Key aspects of the flow include trailing viscous wakes whose strength and location vary with angle of attack, merging wake/boundary layers, different transition phenomena on each of the airfoil elements, boundary-layer separation, and reversed flows in the main element wake. Furthermore, the effects of these physical processes on airfoil performance vary considerably with Reynolds and Mach number.[1,2] Finally, the most important single result of any high-lift wing design study (experimental or otherwise) is necessarily the determination of the maximum lift point itself, since it can play a major role in sizing a transport wing. To the author's knowledge, no fully computational method has been reported that can successfully tackle these problems. In view of the above obstacles to the treatment of practical high-lift systems by numerical analysis, the problem of high-lift configuration design has been largely (almost exclusively) approached empirically. Namely, a three-dimensional high-lift model is designed and tested (at low Reynolds numbers) and the existing data base is updated with any novel results. The testing itself is infrequent (due to high model and testing costs), and the low Reynolds number experimental data obtained has limited applicability to flight Reynolds number.[2] Therefore, even experimental high-lift development programs may not necessarily yield data that can be used to predict flight maximum lift performance.

This article reports on the development of a hybrid method that couples inexpensive-to-run CFD technology with a physical criterion derived from observations made during wind-tunnel testing. This approach has yielded a surprisingly simple, cost-effective, and "design-useful" method for the prediction of maximum lift performance for practical transport wings as a function of Reynolds number. The method is appropriate for configuration development, but should not

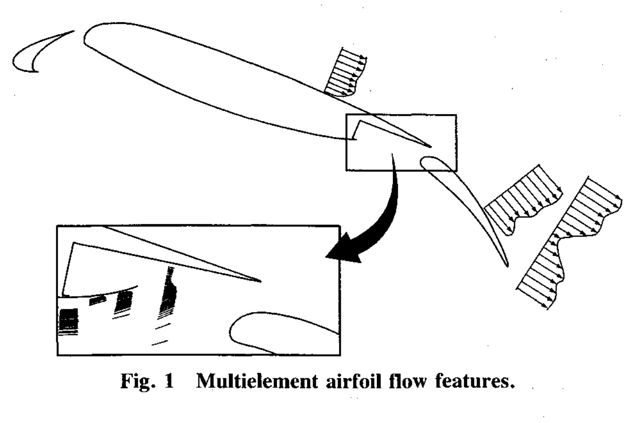

Fig. 1 Multielement airfoil flow features.

be expected to apply to the problem of finding the optimum gap/overhang locations for each of the high-lift wing components; this remains a wind-tunnel testing task and should also be a primary focus for CFD development efforts in this area.

Pressure Difference Rule

For many years, aircraft aerodynamicists have attempted to find empirical means of estimating when a given multielement airfoil achieves its maximum lift condition. Smith[3] reported, e.g., when maximum lift could be expected on a clean airfoil (no high-lift devices) by means of two empirical observations: 1) when the highest local velocities on the airfoil reach a Mach number of 1.0, the limiting airfoil suction peak at maximum lift will be given by the isentropic relation

$$C_p^* = (1/0.7M_\infty^2)\{[(1 + 0.2M_\infty^2)/1.2]^{3.5} - 1\}$$

or, 2) maximum lift will occur when

$$M_\infty^2 C_{p\,\mathrm{peak}} = -1.0$$

This last criterion for maximum lift is also known as Smith's 0.7 "vacuum pressure" relation. However, the 0.7 vacuum pressure relation was based on data obtained beyond Mach 0.4, and this perhaps explains why the relation yields a limiting suction peak of -25 at Mach 0.20. This negative suction peak has, to the authors' knowledge, yet to be measured in the wind tunnel on a transport airfoil at any Reynolds numbers.

The isentropic relation yields $C_p = -13$ for a freestream Mach number of 0.223. This particular value of C_p is similar to minimum suction peaks observed in atmospheric wind-tunnel testing conducted at Mach 0.20 near the maximum lift conditions of airfoils with clean leading edges (no leading-edge device deployed). The criterion for maximum lift of a limiting C_p of -13 has been useful for daily design work, except for the following important drawbacks:

1) It has no dependency on Reynolds or Mach number (parameters known to have a key influence on maximum lift).

2) The criterion is clearly not applicable to airfoils with leading-edge devices where suction peaks as low as -22 have been experimentally observed at the maximum lift condition.

A properly configured multielement airfoil will always stall when either the leading-edge device or the main element has started to stall. The trailing-edge device does not appear to be directly involved in the stall. In fact, the trailing-edge flap tends to be well protected from stalling at high angles of attack. This is because as the geometric angle of attack of the airfoil increases, the actual flap angle of attack decreases (increasing downwash is generated by the forward elements). Hence, it is reasonable to expect that a single empirical correlation could be found that would predict maximum lift on an airfoil having any number of elements, as long as the stall is controlled by any of the forward elements. Close scrutiny of available wind-tunnel data[2] at maximum lift conditions, for single as well as multielement airfoils, revealed a most interesting correlation. Specifically, at a given Reynolds/Mach number combination, there exists a certain pressure difference between the suction peak and trailing edge at the maximum lift condition. For the case of a multielement airfoil, this same rule (referenced here as the pressure difference rule) applies. Thus, at a given freestream Mach number, there is a pressure difference variation with Reynolds number (Fig. 2) that indicates when maximum lift is attained. Again, this correlation applies whether or not the airfoil has an auxiliary leading-edge device. For a multielement airfoil, the pressure difference rule is applied on each of the elements. It is important to note the strong dependency of the pressure difference rule on Reynolds number at the very low Reynolds numbers that can be expected on the outboard sections of most three-dimensional wind-tunnel models tested today.

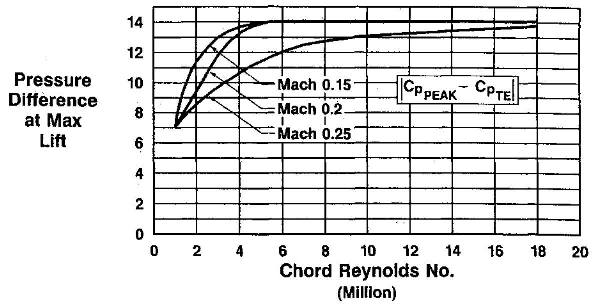

Fig. 2 Pressure difference rule for maximum lift.

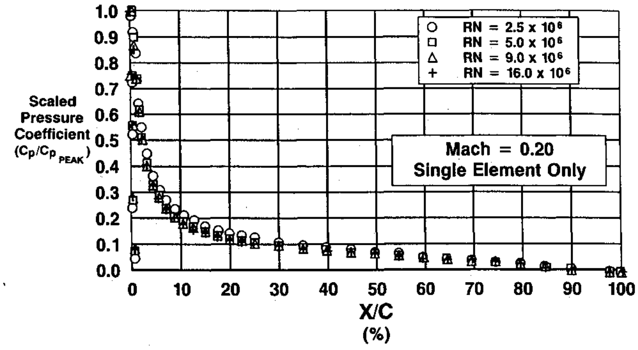

Fig. 3 Scaled pressure distribution on single-element upper surface at maximum lift.

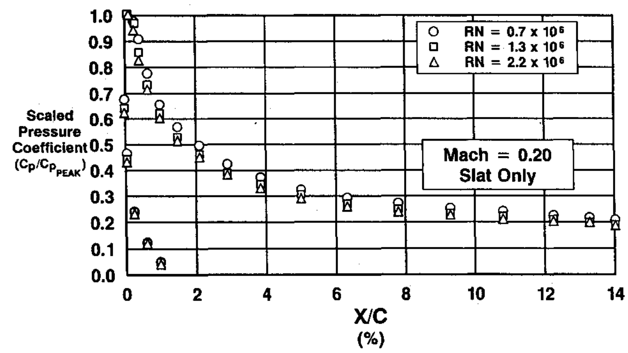

Fig. 4 Scaled pressure distribution on slat upper surface at maximum lift.

While the existence of this so-called pressure difference rule leads directly to a usable criterion for the prediction of the maximum lift condition, a plausible exposition of why this criterion should work for airfoils, regardless of leading-edge configuration, is appropriate. The extensive surface pressure data of Ref. 2 indicated widely varying suction peak levels even on the clean airfoil depending on the freestream condition. Therefore, it was determined (for comparison purposes) to self-scale any chordwise pressure distribution by its corresponding suction peak pressure coefficient. This scaling is similar to the standard canonical pressure form[3] and allows for the one-to-one comparison of the shapes of specific pressure distributions. Scaled pressure distributions for the clean airfoil at the maximum lift condition are shown in Fig. 3. Only the upper surface pressures are shown for clarity. It can be seen that the shapes of the scaled pressure distributions collapse to the same shape beyond chord Reynolds numbers of 5×10^6. This is an interesting finding since the maximum lift capability of this particular airfoil is insensitive to Reynolds number increases beyond 5×10^6.[2] Hence, it appears that the scaled pressure distribution has a limiting shape which is attained at the maximum lift point (this is also the same condition when the pressure difference rule applies). Similarly, scaled pressure coefficients obtained on the slat of a four-element configuration at maximum lift are shown in Fig. 4. Here, the chord has been nondimensionalized with respect to

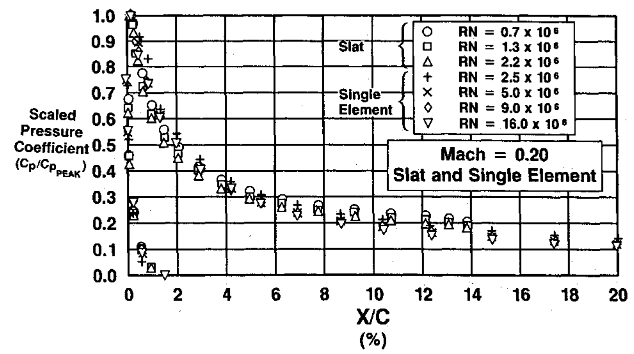

Fig. 5 Scaled pressure distribution on airfoil leading edge at maximum lift.

the clean airfoil, and the Reynolds numbers are based on the slat chord. Again, the scaled pressure curves tend to collapse to a single curve, but some variation due to Reynolds number is apparent. Scaled pressure data at maximum lift for the clean airfoil leading edge and the slat of the multielement airfoil are shown for a variety of Reynolds numbers in Fig. 5. It can be seen that all curves tend to collapse to the same curve (with some variation with Reynolds number) whether or not the airfoil has a slat. This is a remarkable result, since it quantitatively shows that the maximum lift performance of a slatted multielement airfoil is limited in an absolute sense by the clean airfoil leading-edge shape. In other words, even though the slat is in an upwash/downwash situation, in spite of slat trailing-edge dumping velocity effects[3] which distort the pressure distribution over the slat, and in spite of whatever other flow complications, the configuration with a slat will yield scaled pressure results essentially identical to those obtained with the clean leading edge. Therefore, it is not unreasonable to expect that a single criterion such as the pressure difference rule would apply to either.

Results

For the calculation of three-dimensional maximum lift, the assumption is made that the pressure difference rule discussed above can be applied directly, even though it is derived from two-dimensional data. It is recognized that a wing will experience the well-known pressure relief effect and will thus have a more positive suction peak for a given angle of attack than a corresponding two-dimensional airfoil. However, it is expected that the wing will attain the same suction peak (at a higher angle of attack) at its critical stall station as it would in two-dimensional flow for the equivalent airfoil section. This seems intuitive enough, at least for high-aspect ratio wings such as those found on transport aircraft. The maximum lift condition is predicted to occur when the computed pressure difference anywhere along the wing span matches that indicated by the curve of Fig. 2.

The application of the pressure difference rule is very straightforward:

1) Computed flow solutions are obtained at various angles of attack for the desired geometry. Surface panel method technology is not only sufficient for this step, but is really the only cost- and time-effective way to generate the solutions. The Douglas higher-order surface panel method[4] was used for the studies presented here, but any other reliable method can be substituted. Sufficient surface paneling should be provided to ensure adequate definition at the leading and trailing edges.

2) For a given freestream Reynolds number and Mach number, an allowable pressure difference distribution vs span is constructed from Fig. 2, based on the wing chord distribution.

3) It is graphically determined at what spanwise wing station and wing lift coefficient the computational results match the curve constructed in step 2.

Method Validation with Royal Aircraft Establishment Data

The three-dimensional Royal Aircraft Establishment (RAE) experimental data base[5] was selected for verification of the present maximum lift prediction method based on the new pressure difference rule. This data base is ideal for initial method validation because of its systematic buildup of high-lift system complexity. The experiments were conducted in the RAE 11.5- by 8.5-ft low-speed wind tunnel. The model had an aspect ratio of 8.35 and wing quarter-chord sweep of 28 deg, with a taper ratio of 0.35. The high-lift system included a 16% chord leading-edge slat (15, 20, and 25 deg) and a 34% Fowler flap (10, 25, and 40 deg). The test was conducted transition-free at a Reynolds number of 1.35×10^6 based on the mean wing chord and the nominal Mach number of 0.22.

The pressure difference rule was used to predict $C_{L\max}$ for the RAE wing configurations listed in Table 1. Gaps and overhangs were as reported in Ref. 5.

Application of the pressure difference rule is simple. First, the Reynolds number variation along the span is calculated, this is a function of clean wing chord only. Specifically, for the RAE wing this becomes

$$R_N(\eta) = (0.381 - 0.24765\eta)(1.35 \times 10^6)/0.257175$$

where $\eta = 0 \rightarrow 1.0$

$$R_N(0.3) = 1.61 \times 10^6$$

$$R_N(0.76) = 1.01 \times 10^6$$

While only two points are needed to define the Reynolds number variation vs span for this simple planform, a point will be needed at each planform break in addition to the root and the tip. The pressure difference that can be expected at maximum lift at $R_N = 1.61 \times 10^6$ and 1.01×10^6 (interpolate for $M_\infty = 0.22$ data) is obtained from Fig. 2. Hence, at the 30% spanwise location, $|\Delta C_p| = 8.2$ is indicated, and at the 76% spanwise location, $|\Delta C_p| = 7$. A straight line connecting these two points represents the boundary that predicts when $C_{L\max}$ occurs. This boundary will not be different for a clean wing or for a multielement, so it can be used for all subsequent $C_{L\max}$ studies on this wing, as long as the spanwise distribution of wing chord of the clean wing does not change.

The results for panel method solutions at 11.84 and 12.84 deg, as well as the pressure difference to be expected at maximum lift, are plotted in Fig. 6. Linear interpolation yields a predicted $C_{L\max}$ of 1.04, and the critical spanwise station is identified at 87% of the span. The pressure difference rule was then similarly applied to the flapped wing geometries shown in Fig. 7, and the corresponding lift curves with the predicted $C_{L\max}$ points are displayed in Fig. 8. For these flapped cases the flap has been underdeflected, using the schedule shown in Fig. 9, to roughly account for the known decambering effect of the boundary layer and wakes on a multielement wing. Agreement between experiment and prediction is seen to be very good throughout each lift curve, up to and

Table 1 RAE wing configuration

Leading edge	Trailing edge
Clean	Clean
Clean	δ_f = 10 deg
Clean	δ_f = 25 deg
Clean	δ_f = 40 deg
δ_s = 15 deg	Clean
δ_s = 25 deg	Clean
δ_s = 25 deg	δ_f = 10 deg
δ_s = 25 deg	δ_f = 25 deg (span = 100%, 80%, 60%)
δ_s = 25 deg	δ_f = 40 deg

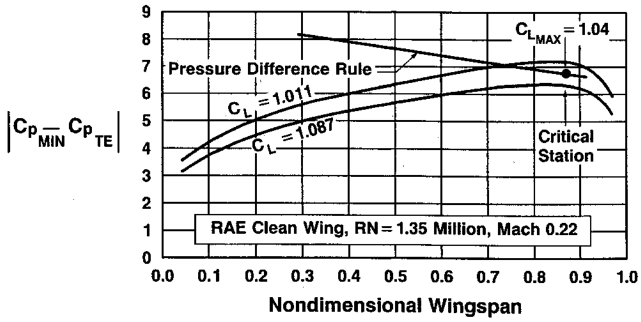

Fig. 6 Maximum lift prediction by pressure difference rule.

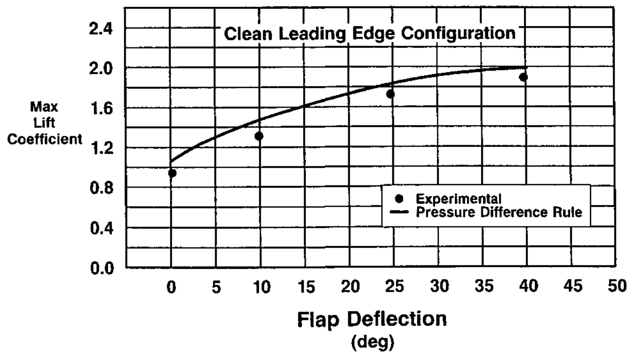

Fig. 10 Effect of flap deflection on maximum lift.

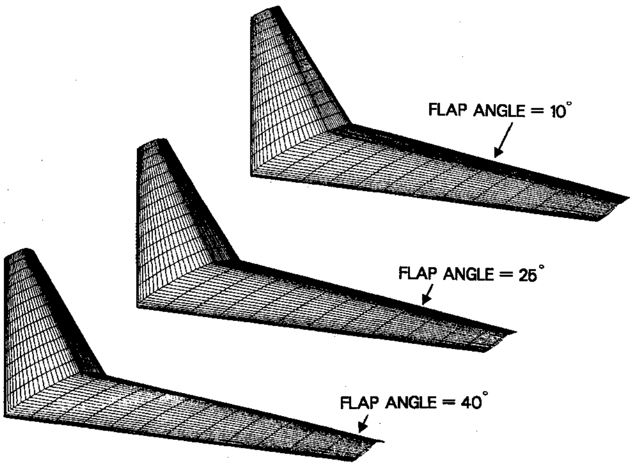

Fig. 7 Geometries for RAE wing with flap.

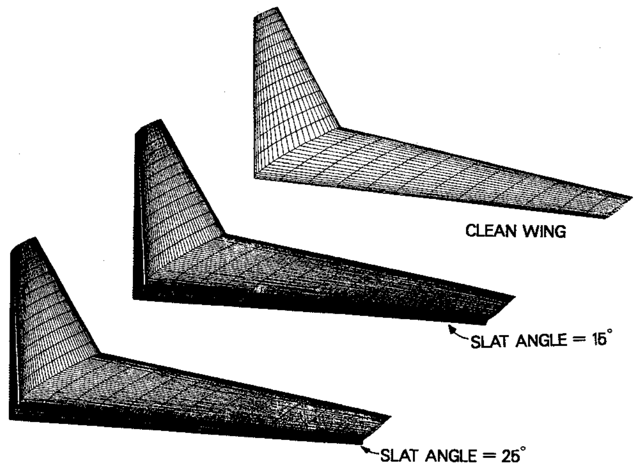

Fig. 11 Geometries for RAE wing with slat.

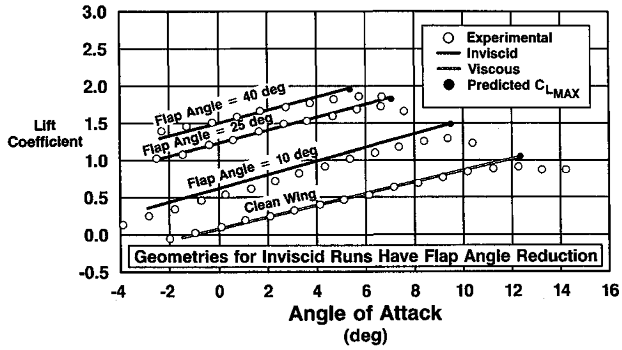

Fig. 8 Lift curves for RAE wing with flap.

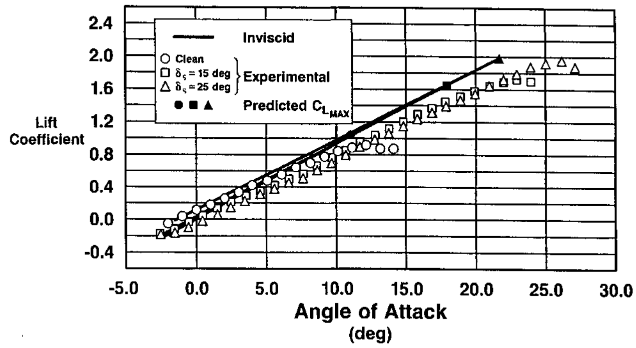

Fig. 12 Lift curves for RAE wing with slat.

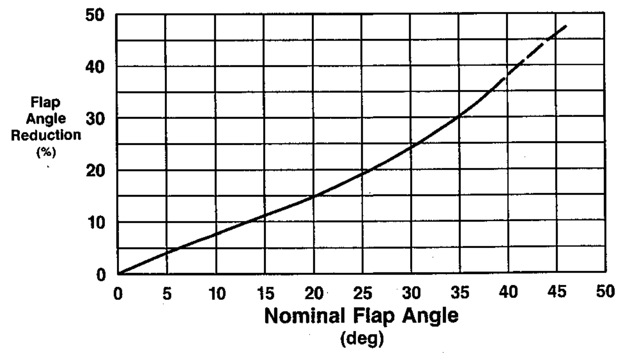

Fig. 9 Flap angle relaxation curve.

including, $C_{L\max}$. The effect of flap deflection on maximum lift for this clean leading-edge configuration is shown in Fig. 10, where the present $C_{L\max}$ method correctly indicates small lift improvements in going from 25- to 40-deg flaps for this particular wing; this is a key result, because with this information it would be difficult to consider the 40-deg flaps desirable, given the likelihood of substantial drag for the minimal improvement in lift. It is also worth noting that the predicted flap lift increments shown in Fig. 8, over the positive angle-of-attack range, are accurate enough to provide a substantial capability for early loads prediction for new wing designs not yet wind-tunnel tested. It is emphasized here that the flap reduction curve of Fig. 9 is based on relatively low Reynolds number data, and modifications to the curve (perhaps a family of curves) should be apparent as high Reynolds number three-dimensional data become available.

Results for the slatted configurations illustrated in Fig. 11 are shown in Fig. 12. As expected, the inviscid calculations overpredict the overall level and slope of the lift curves, but the prediction of maximum lift as a function of slat deflection using the pressure difference rule is quite satisfactory (Fig. 13).

Geometries for slat/wing/flap configurations are shown in Fig. 14. The slat deflection is 25 deg and flap angles are 10, 25, and 40 deg covering the range from takeoff to landing. The computed lift curves, including the predicted $C_{L\max}$ using the pressure difference rule, are shown in Fig. 15. The predicted variation of maximum lift vs flap deflection is summarized in Fig. 16. A maximum lift buildup is shown in Fig. 17. Here, good agreement is shown between the present method

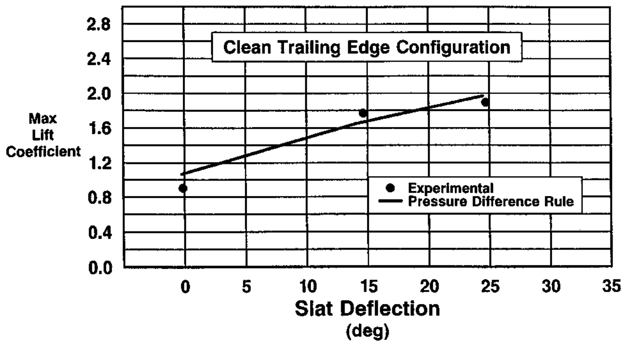

Fig. 13 Effect of slat deflection on maximum lift.

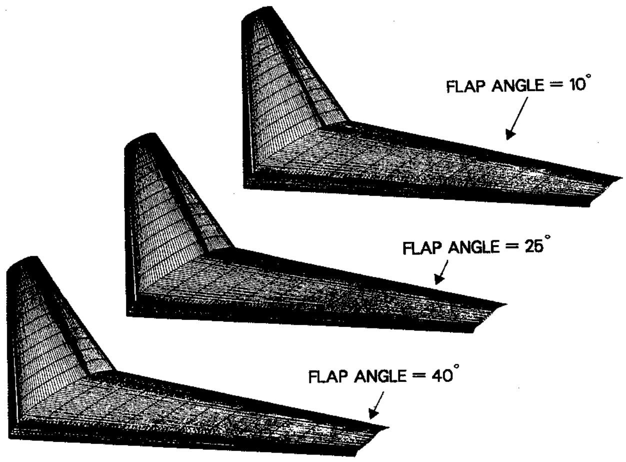

Fig. 14 Geometries for RAE wing with slat and flap.

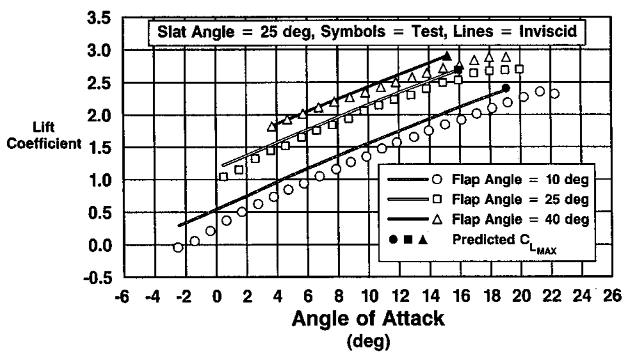

Fig. 15 Lift curves for RAE wing with slat and flap.

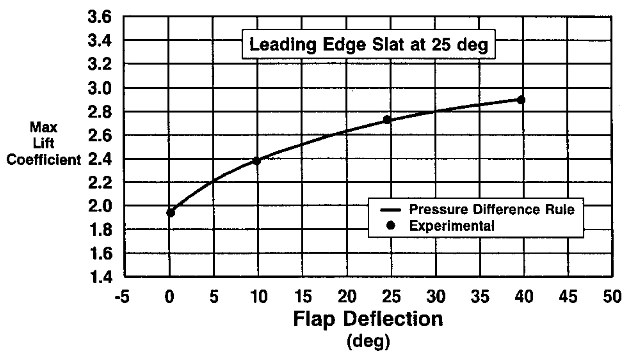

Fig. 16 Effect of flap deflection on maximum lift for RAE wing with slat.

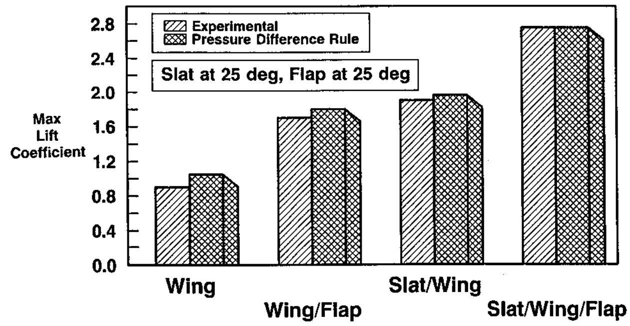

Fig. 17 Maximum lift buildup for RAE wing.

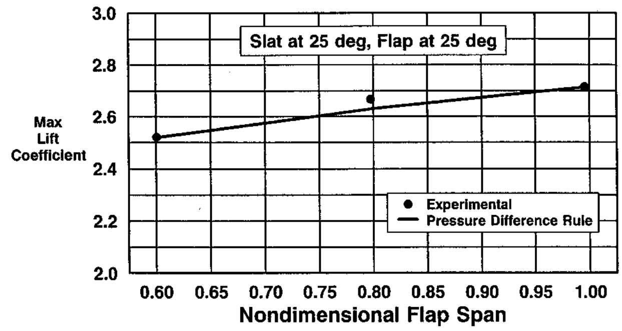

Fig. 18 Effect of flap span on maximum lift.

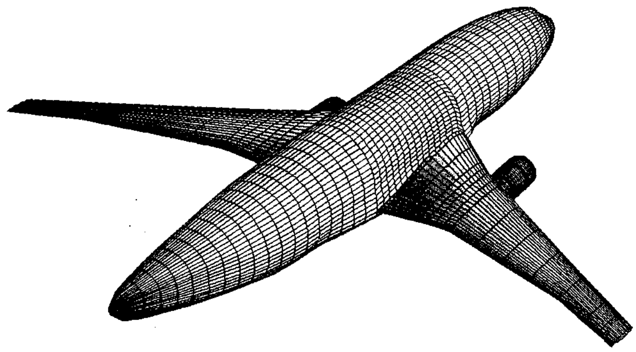

Fig. 19 EET wing/body/nacelle/pylon geometry.

and experiment for both the absolute values of maximum lift and the increments between candidate configurations. Results for the effect of flap span on maximum lift are shown in Fig. 18.

Reynolds Number Trends

Further applications of the pressure difference rule were made to a more recent data base obtained at the NASA Ames 12-ft wind tunnel. This model was used in joint tests between Douglas Aircraft and NASA as part of the energy efficient transport (EET) program during the late 1970s. The model was representative of a new transport design, and had a quarter-chord sweep of 28.5 deg, an aspect ratio of 10.502, and a taper ratio of 0.1407.

Reynolds numbers based on the mean aerodynamic chord as high as 5.12×10^6 were possible at 0.20 Mach number. The test was conducted transition-free.

Figure 20 summarizes the results obtained with the present method for the wing/body/nacelle/pylon configuration of Fig. 19. The agreement between predicted and measured maximum lift coefficient as a function of Reynolds number is remarkable. Furthermore, the method indicates that a further gain of 0.20+ in $C_{L_{\max}}$ can be expected at the flight Reynolds number (15×10^6) for this wing. Predicted and measured $C_{L_{\max}}$ vs Reynolds number curves at Mach 0.20 are shown in Fig. 21 for the full-blown landing geometry of Fig. 22. The configuration consisted of a wing/body/nacelle/pylon with

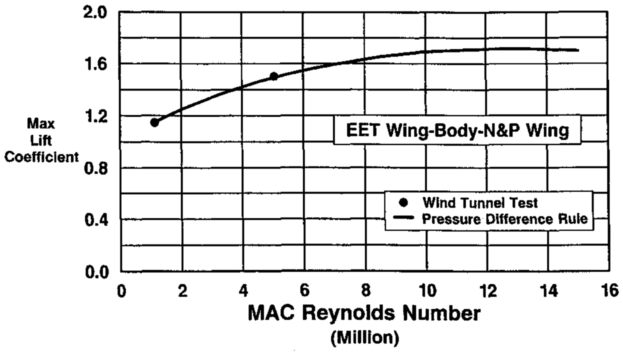

Fig. 20 Reynolds number effect on maximum lift for EET wing/body/nacelle/pylon.

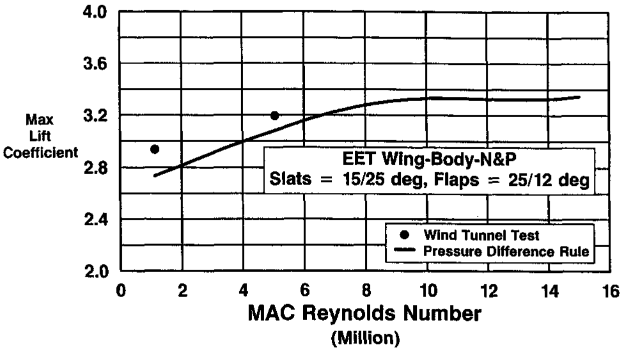

Fig. 21 Reynolds number effect on maximum lift for EET landing configuration.

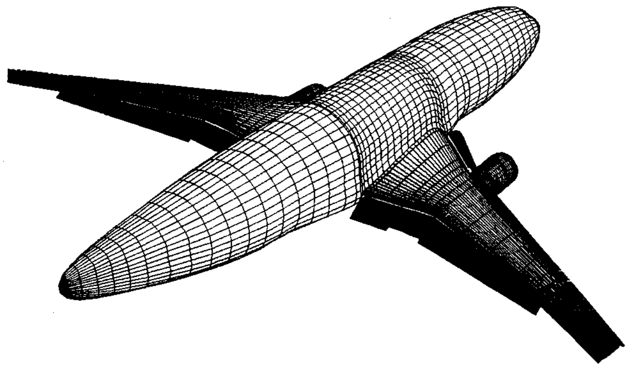

Fig. 22 EET model configured for landing.

leading-edge slats at 15 deg/25 deg (inboard/outboard), two-segment flaps deflected 25 deg/35 deg, and a flaperon deflected 25 deg. Again, the method captures the measured trend with Reynolds number for the two Reynolds numbers tested. The predictions also indicate a gain of 0.20+ in $C_{L\max}$ at the flight Reynolds number.

It is worth noting here, that while the wind-tunnel model was outfitted with inboard nacelle strakes to control the stall, as is customary on today's airplanes, the strakes were not a factor in the tunnel. The very low tolerance to high suction peaks due to the low local Reynolds numbers caused the outboard wing to stall first. That this should be the case is intuitively obvious from Fig. 2. The pressure difference capability at the outboard region of a highly tapered wing tested at 5.12×10^6 can be as little as half as that at the wing mean aerodynamic chord (MAC). Since the wing MAC is outboard of the pylon/wing intersection where there is a small (but very important) unprotected leading-edge region, in the tunnel the outboard is guaranteed to stall prior to the unprotected wing leading-edge region inboard of the pylon. Therefore, fortuitously enough, even though the wind-tunnel model had nacelle strakes, they did not play a role in the stall and they need not be modeled numerically.

Additional results were obtained for the current narrow-body transport shown in Fig. 23. The wing is configured for landing with both leading- and trailing-edge devices deployed. The variation of 1 g $C_{L\max}$ with Reynolds number for this configuration is shown in Fig. 24. The predictions compare very well with available wind-tunnel and flight test results. It can be seen again that the variation with Reynolds number is considerable, and the present method captures it remarkably well.

Further predictions were obtained for the wide body landing configuration of Fig. 25. This particular geometry is extremely complicated. The configuration has fan and core cowls, pylon, upper and lower winglets, differentially deflected slats, slotted flaps separated by the high-speed aileron, and a fuselage. To the credit of panel method developers,[4] the capability to successfully obtain an inviscid solution on this aircraft geometry configured for landing is a feat in itself. Results for the wide-body transport are shown in Fig. 26. Here, the variation of $C_{L\max}$ vs Reynolds number is significant, but not as pronounced as it is for the narrow-body aircraft having a

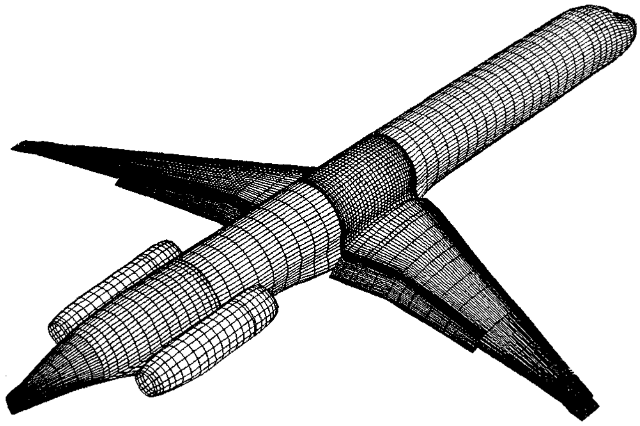

Fig. 23 Twin-jet transport configured for landing.

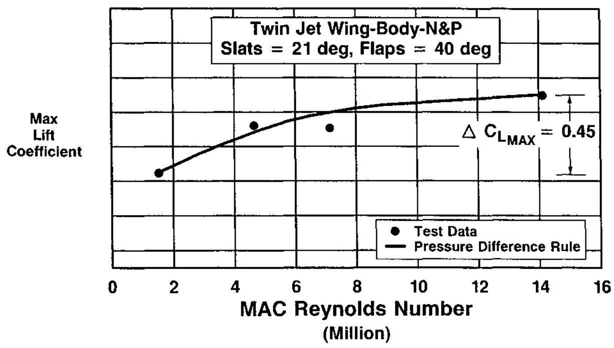

Fig. 24 Effect of Reynolds number on twin-jet transport.

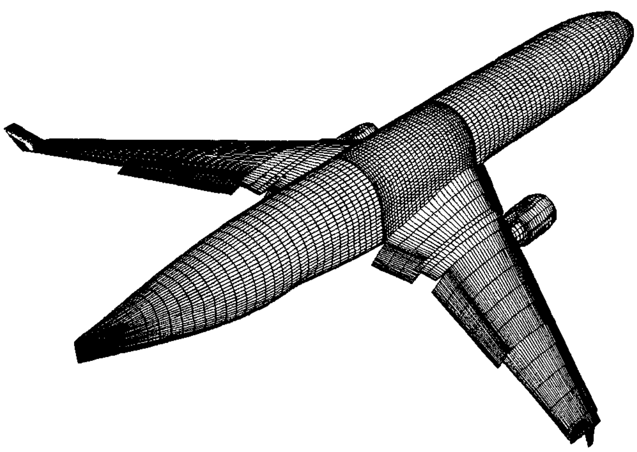

Fig. 25 Trijet transport configured for landing.

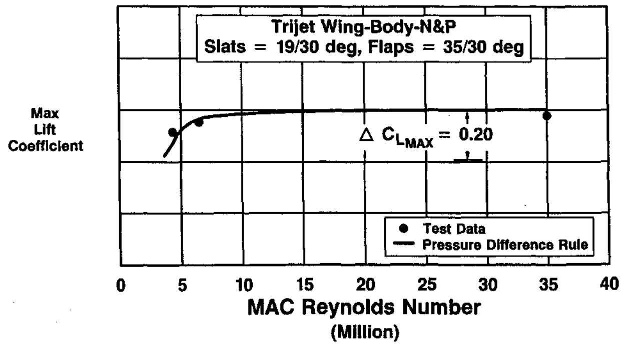

Fig. 26 Effect of Reynolds number on trijet configured for landing.

lower wing taper ratio which coupled with a lower flight Reynolds number leads to increased susceptibility to the Reynolds number trend of Fig. 2.

Conclusions

A new semiempirical three-dimensional $C_{L\,\max}$ method for multielement transport wings has been described. The method is based on cost-effective and reliable CFD technology (surface panel methods), and the newly developed pressure difference rule which identifies when the maximum lift condition has been achieved as a function of Reynolds and Mach number. Predictions from the present method agree remarkably well with available wind-tunnel and flight test data, and the method is simple to use. The present method has been demonstrated to represent a substantial advancement in predictive capability for design studies of transport high-lift wing configurations at maximum lift conditions.

References

[1]Fiddes, S. P., Kirby, D. A., Woodward, D. S., and Peckham, D. H., "Investigations into the Effects of Scale and Compressibility on Lift and Drag in the RAE 5m Pressurized Low-Speed Wind Tunnel," *Aeronautical Journal*, Vol. 89, Paper 1302, March 1985, pp. 93–108.

[2]Valarezo, W. O., Dominik, C. J., McGhee, R. J., Goodman, W. L., and Paschal, K. B., "Multi-Element Airfoil Optimization for Maximum Lift at High Reynolds Numbers," AIAA Paper 91-3332, Sept. 1991.

[3]Smith, A. M. O., "High-Lift Aerodynamics," AIAA Paper 74-939, Aug. 1974.

[4]Hess, J. L., Friedman, D. M., and Clark, R. W., "Calculation of Compressible Flow About Three-Dimensional Inlets with Auxiliary Inlets, Slats, and Vanes by Means of a Panel Method," McDonnell Douglas Rept. MDC J3789, June 1985; see also AIAA Paper 85-1196, 1985 and NASA CR-174975, June 1985.

[5]Lovell, D. A., "A Wind-Tunnel Investigation of the Effects of Flap Span and Deflection Angle, Wing Planform and a Body on the High-Lift Performance of a 28° Swept Wing," Aeronautical Research Council, C.P. 1372, London, 1977.

[6]Oliver, W. R., "Results of Design Studies and Wind Tunnel Tests of an Advanced High-Lift System for an Energy Efficient Transport," NASA CR-159389, Dec. 1980.